Testing, numerical modelling and design of S690 high strength steel welded I-section stub columns

Yao Sun [a], Yating Liang [b], Ou Zhao [*a]

[a] School of Civil and Environmental Engineering, Nanyang Technological University, Singapore

[b] School of Engineering, University of Glasgow, Glasgow, UK

[*] Corresponding author, Phone: +65 6790 6934

Email: ou.zhao@ntu.edu.sg

Abstract

This paper describes a comprehensive testing and numerical simulation investigation into the material properties, membrane residual stresses and compression capacities of S690 high strength steel welded I-section stub columns. The testing programme was performed on eight welded I-sections fabricated from 5 mm thick S700MC high strength steel hot-rolled plates by means of gas metal arc welding, and included material tensile coupon tests, membrane residual stress measurements, initial local geometric imperfection measurements, and sixteen concentrically loaded stub column tests. A membrane residual stress distribution model for S690 high strength steel welded I-sections was firstly proposed, based on the experimentally measured results. In conjunction with the structural testing, a numerical modelling study was carried out, in which finite element models were initially developed and validated against the experimental results, and afterwards employed to conduct parametric studies, aiming at generating further structural performance data over a broader range of cross-section sizes. The

obtained experimental and numerical data were used to evaluate the accuracy of the slenderness limits (for classifications of plate elements and cross-sections) and design rules for S690 high strength steel welded I-section stub columns, as set out in the European, American and Australian standards. The results of the evaluation revealed that the codified slenderness limits are accurate for the plate element and cross-section classifications of S690 welded I-sections in compression, and the established local buckling design provisions in the considered three codes result in precise and consistent cross-section compression resistance predictions for both non-slender and slender S690 welded I-section stub columns.

Keywords: Design analysis; Design standards; Grade S690 high strength steel; Local stability; Membrane residual stress measurements; Numerical simulation; Stub column tests; Parametric studies; Welded I-sections

1. Introduction

Growing emphasis is being placed on the use of high strength construction materials in structural and bridge engineering [1–3], in order to adapt to the increasing need for high-rise buildings and long-span bridges in the past decade. Compared with the conventional mill steel grades S235, S275 and S355 with the nominal yield stresses less than or equal to 355 MPa, high strength steel grade S690 possesses substantially more superior mechanical strength with the nominal yield stress of 690 MPa. Therefore, the use of S690 high strength steel in construction enables the achievement of structural members designed with smaller cross-

section sizes and lighter weights, which not only facilitate the transportation and assembly of the components, but also result in more usable interior space and lighter self-weight of the structure. Although the advantages of using high strength steel in construction have been highly acknowledged, its actual application is generally hindered by the lack of suitable design guidelines, since most of the formulations and provisions set out in the exiting design standards for high strength steel structures were developed by directly mirroring those for normal strength mild steels. This has thus prompted in-depth research to investigate the behaviour of different types of high strength steel structural components, quantify their load-carrying capacities and derive more efficient and accurate design rules. A brief review of the previous experimental and numerical studies of S690 high strength steel welded I-section structural members is provided herein. Rasmussen and Hancock [4] performed stub column tests on S690 welded I-sections to investigate their local buckling responses and compression resistances, while the flexural buckling behaviour and strengths of S690 welded I-section long columns were experimentally and numerically studied in [5–9]. Ma et al. [10,11] carried out a testing and numerical simulation programme to examine the global stability of S690 welded I-section beam-columns subject to combined compression and bending. The brief review generally indicated that although there have been extensive studies on the member stability of S690 high strength steel welded I-section long columns and beam-columns, investigations into the local buckling behaviour of S690 welded I-section stub columns remain scarce, with the only study reported by Rasmussen and Hancock [4] in the early 1990s, and, to date, membrane residual stresses in S690 welded I-sections have not been measured. This thus prompted the present research, to further investigate the local stability and compressive load-carrying capacities of

S690 high strength steel welded I-section stub columns and experimentally verify the membrane residual stress amplitudes and distributions in S690 high strength steel welded I-sections.

In the present paper, a comprehensive experimental programme, including material tensile coupon tests, membrane residual stress and initial local geometric imperfection measurements, and sixteen concentrically loaded stub column tests on eight S690 welded-I sections, was firstly conducted. The experimental investigation was supplemented by a finite element modelling study, where numerical models were initially developed to simulate the experimentally observed results and subsequently adopted to conduct parametric studies to generate additional numerical data. Finally, the experimentally and numerically derived results were employed to assess the accuracy of the local buckling design rules for S690 high strength steel welded I-section stub columns set out in the European code EN 1993-1-12 [12], American specification ANSI/AISC 360-16 [13] and Australian standard AS 4100 [14].

2. Experimental investigation

2.1. General

A structural testing programme was carried out to study the material properties, membrane residual stresses and compression capacities of S690 high strength steel welded I-sections. Eight I-section sizes – I-50×50×5, I-70×70×5, I-80×60×5, I-90×70×5, I-100×100×5, I-

140×70×5, I-150×150×5 and I-200×100×5 – were considered in the present experimental study, and all the I-sections were fabricated from the same batch of 5 mm thick S700MC high strength steel hot-rolled plates by means of gas metal arc welding (GMAW). Overall, the testing programme involved material tensile coupon tests to obtain the stress–strain responses of the examined S690 high strength steel, residual stress measurements to determine the membrane residual stress magnitudes and distributions in S690 welded I-sections, imperfection measurements to derive the initial local geometric imperfections of the stub column specimens, and concentric compression tests to investigate the local stability and compression resistances of welded I-section stub columns in grade S690 high strength steel.

2.2. Material testing

Material testing was firstly conducted to derive the material stress–strain responses of the studied S690 high strength steel welded I-sections. Tensile coupons were extracted from the same batch of plates as that used in the fabrication of the welded I-section stub column specimens. Specifically, two longitudinal coupons were cut along the rolling direction of the plate, while two additional transverse coupons were extracted perpendicularly to the plate rolling direction. The dimensions of the two pairs of coupons are in compliance with the geometric requirements specified in EN ISO 6892-1 [15]. A Schenck 250 kN hydraulic testing machine, driven by displacement control, was utilised to perform tensile coupon tests, with the applied loading rates respectively set to be equal to 0.05 mm/min and 0.8 mm/min up to and beyond the nominal yield stress of 690 MPa. The resulting strain rates satisfied the relevant

requirements given in EN ISO 6892-1 [15]. Fig. 1 displays the setup for tensile coupon tests, including an extensometer mounted onto the central 50 mm of the necked portion of the coupon and a pair of the strain gauges attached to the two parallel wider faces of the coupon at mid-height. Fig. 2 shows the stress–strain curves measured from both the longitudinal and transverse coupons, whilst the key average measured material properties, including the Young's modulus E, the yield stress f_y, the ultimate stress f_u, the ultimate-to-yield stress ratio f_u/f_y, the strain at the ultimate stress ε_u, and the fracture strain measured over the standard gauge length of 50 mm ε_f, are reported in Table 1. It is worth noting that the stress–strain curves of high strength steel grade S690 display much shorter yield plateaux and lower levels of material strain hardening and ductility (as also reflected by the ratios of f_u/f_y and ε_u in Table 1), compared to those shown by its normal strength mild steel counterparts.

2.3. Membrane residual stress measurements

Membrane residual stresses are introduced into welded steel sections during the welding process, which can lead to premature failure of the structural components. Measurements on the magnitudes and distributions of membrane residual stresses in S690 high strength steel welded I-sections were therefore performed and reported herein. The sectioning method was employed for the membrane residual stress measurements on two S690 welded I-sections I-150×150×5 and I-200×100×5, with the procedures conforming to those specified in Ziemian [16]. The dimensions and locations of the strips sectioned for the membrane residual stress measurements are depicted in Figs 3 and 4. For each strip, the nominal length and width are

equal to 150 mm and 10 mm, respectively. Prior to sectioning, an automatic dot puncher was used to drill a pair of gauge holes (1.98 mm in diameter), located along the centreline of the outer face of each strip and at a distance of 25 mm from the strip ends; this resulted in the nominal strip length between each pair of gauge holes L_0 equal to 100 mm, while the actual length of each strip was measured by means of a Demec gauge with 100 mm gauge length. Membrane residual stresses were then released by sectioning the welded I-section specimens into strips. This was achieved through the use of a waterjet cutting machine, which induced very little if any heat input into the strips during the cutting process, and thus did not affect their original membrane stress patterns and amplitudes. Fig. 5 depicts a typical sectioned S690 welded I-section (I-200×100×5). The length between gauge holes for each strip after sectioning was again measured by the Demec gauge. The effect of temperature variation on the change in strip length during the membrane residual stress measurements was taken into account by means of a temperature reference bar, which was extracted from the same batch of S700MC plates as that utilised in the fabrication of welded I-sections. The temperature reference bar was drilled with two gauge holes, between which the length was measured before and after sectioning through the use of the Demec gauge.

The relieved axial strains ε_0 resulted from the release of membrane residual stresses can be derived from Eq. (1), where r_1 and t_1 are respectively the lengths of the strip and temperature reference bar, measured by the Demec gauge before sectioning of the I-section specimens, whilst r_2 and t_2 are the measured lengths of the strip and temperature reference bar after sectioning, respectively. It is worth noting that positive and negative values calculated from Eq.

(1) respectively signify the release of tensile and compressive strains upon sectioning of the welded I-sections. As obtained from previous residual stress measurements on normal strength mild steel [17,18] and stainless steel [19,20] welded sections and also observed in the present measurements on S690 high strength steel welded I-sections, the sectioned strips in the vicinity of welds displayed slightly curved shapes; this can be attributed to the existence of a relatively high level of through-thickness bending residual stresses near the welds, and corrections to the relieved axial strains calculated from Eq. (1) were then made on the basis of Eq. (2) [17], where $\varepsilon_{0,c}$ is the corrected relieved axial strain and δ is the maximum deviation from a straight reference line connecting the two gauge holes of the strip. The released membrane residual stresses can then be back-calculated as the products of the relived axial strains ε_0 (or $\varepsilon_{0,c}$) and the Young's modulus E; negative and positive values indicate compressive and tensile residual stresses, respectively.

$$\varepsilon_0 = \frac{(r_1 - t_1) - (r_2 - t_2)}{L_0 + (r_1 - t_1)} \tag{1}$$

$$\varepsilon_{0,c} = \varepsilon_0 + \frac{(\delta / L_0)^2}{6(\delta / L_0)^4 + 1} \tag{2}$$

The magnitudes and distributions of the experimentally derived membrane residual stresses for the two S690 welded I-sections I-200×100×5 and I-150×150×5 are exhibited in Figs 6(a) and 6(b), respectively, while the peak values of both the acquired tensile and compressive residual stresses, normalised by the material yield stress f_y measured from the longitudinal coupons, are presented in Table 2, where the subscripts 't' and 'c' respectively indicate tensile and compressive residual stresses, and the subscripts 'f' and 'w' respectively denote flange and web.

Given that there have been no codified membrane residual stress distribution models for high strength steel welded sections, the corresponding predictive models for normal strength mild steel welded I-sections, as specified in the European convention ECSS [21] and Swedish regulations BSK 99 [22], were assessed herein for their applicability to S690 high strength steel welded I-sections. The two codified residual stress predictive modes for normal strength mild steel welded I-sections were established based on the same distribution pattern, as shown in Fig. 7, but with different distribution coefficients (a, b, c and d) and peak compressive residual stresses (f_{fc} and f_{wc}), as presented in Table 3. A graphic comparison between the measured membrane residual stresses and the two predictive models given in ECSS [21] and BSK 99 [22] is depicted in Figs 8(a) and 8(b); note that the measured residual stress data points were plotted in a normalised format, with the normalised positions at 0.0 (origin point) and 1.0 (end point) respectively representing the web-to-flange junction and the mid-point of the web or the tip of the flange. The comparison results showed that the two codified predictive models generally over-predict the peak tensile residual stresses but result in underestimated peak compressive residual stresses for S690 high strength steel welded I-sections. It is also evident in Fig. 8 that the transition regions of the membrane residual stresses in S690 high strength steel welded I-sections were considerably wider when compared to those specified by the two codified predictive models for normal strength mild steel welded I-sections. This thus prompted the development of a new predictive model specific for the membrane residual stresses in S690 high strength steel welded I-sections herein. The new membrane residual stress predictive model follows the general pattern depicted in Fig. 7, but employs a new set of distribution coefficients as well as different peak residual stress amplitudes. Fig. 8 shows a comparison of

the new residual stress predictive model with the measured membrane residual stresses in S690 high strength steel welded I-sections, indicating good agreement.

2.4. Initial local geometric imperfection measurements

Initial local geometric imperfections affect the local stability and load-carrying capacities of thin-walled steel section structural components, and were thus measured for all the S690 high strength steel welded I-section stub column specimens herein. The experimental rig for initial local geometric imperfection measurements is similar to that utilised by Schafer and Peköz [23] and shown in Fig. 9, where an LVDT is mounted onto the head of a milling machine with the specimen lying on the base table of the machine. Three local imperfection measurements were carried out on each constituent plate element of the S690 welded I-section. Specifically, for the internal web, measurements were carried out along the centreline and the two edges of the web-to-flange junctions, while for the outstand flange, measurements were conducted along the centreline and the two flange tips, as depicted in Fig. 10. It is also worth noting that imperfection measurements were all carried out over the central 75% of the specimen lengths, in order to eliminate the effect of flaring of specimen ends upon cutting. The initial local geometric imperfections along each measured line were defined as the deviations from a linear regression line fitted to the measured data set [24–28], with the maximum amplitude denoted as ω_n, in which the subscript 'n' indicates the measured line. The initial local geometric imperfection amplitudes of the web and two flanges (ω_w, ω_{f1} and ω_{f2}) were taken as the largest values from the three measurements on the respective plate elements, as reported in Table 4,

while the initial geometric imperfection amplitude of the specimen ω_0 was taken as the maximum of ω_w, ω_{f1} and ω_{f2}.

2.5. Stub column tests

For each of the eight S690 high strength steel welded I-sections, two repeated stub column tests were carried out, to investigate its local stability and compression resistance under compression. The nominal length of each stub column specimen was taken as the minimum of three times the outer section depth and twenty times the radius of gyration about the minor principal axis [16]; each selected nominal specimen length was deemed long enough to include a representative distribution pattern of membrane residual stress and initial local geometric imperfection, but still short enough to prevent column flexural buckling. The measured member length and cross-section sizes of each S690 high strength steel welded I-section stub column specimen are summarised in Table 4, in which L is the specimen length, b_f is the flange width, h is outer section depth and t is the material thickness. Prior to stub column tests, milling and deburring were carried out on the specimen ends; this enabled the achievement of flat end surfaces of the specimens and thus uniformly distributed compressive stresses over the full cross-sections during testing. All the stub column specimens were compressed between the fixed end platens of an Instron 2000 kN hydraulic testing machine at a constant loading speed of 0.3 mm/min. Fig. 11 depicts the stub column test setup, including a pair of longitudinally-placed LVDTs to measure the end shortening of the specimen, and two strain gauges, attached to the web-to-flange junctions of the specimen at mid-height, to record the axial strains. The

end shortening values derived from the LVDTs were modified by eliminating the elastic deformation of the end platens of the testing machine based on the strain gauge readings [25,28–31]. The modified load–end shortening curves for all the sixteen tested S690 high strength steel welded I-section stub columns are presented in Fig. 12, while the key experimental results, including the ultimate load N_u, the end shortening at failure δ_u, and the ultimate-to-yield load ratio $N_u/(Af_y)$, in which A is gross cross-section area, are presented in Table 5. All the tested S690 welded I-section stub columns were shown to fail by local buckling, and Fig. 13 displays typical failure modes of the specimens I-150×150×5-1, I-90×70×5-1 and I-200×100×5-1 with cross-section aspect ratios h/b varying between 1.0 and 2.0.

3. Numerical study

3.1. General

In parallel with the testing programme, a numerical simulation programme, including a validation study and a parametric study, was conducted by means of the finite element (FE) analysis software ABAQUS [32]. In the numerical validation study, FE models were developed and validated against the experimentally obtained results, while in the numerical parametric study, the validated FE models were utilised to generate further numerical data to supplement the derived test results.

3.2. Development of finite element models

The shell element S4R [32] has been extensively used in previous numerical modelling of welded I-section steel components [11,19,33,34], and was also employed herein for simulating the S690 high strength steel welded I-section stub columns. For the purpose of selecting suitable shell element size, a mesh sensitivity study, considering a series of element sizes varying between 0.5t and 4t, was performed. The results of the mesh sensitivity study generally indicated that an element size equal to the material thickness t was capable of well incorporating the membrane residual stress distributions into the FE models and meanwhile providing both computational accuracy and efficiency. This element size was thus used for discretisation of the welded I-section stub column FE models herein. Regarding the material modelling of grade S690 high strength steel, the plastic material model with isotropic hardening, as provided in ABAQUS [32], requires the inputted material properties to be specified in the form of true stress and true plastic strain. Therefore, the stress−strain curves, measured from the longitudinal coupons, were firstly converted into the true stress−true plastic strain responses and then incorporated into ABAQUS [32]. Membrane residual stresses for S690 welded I-sections, as derived from the predictive model proposed in Section 2.3, were incorporated into the finite element models through the '*INITIAL CONDITIONS' command. Fig. 14 shows a typical residual stress distribution incorporated into the finite element models for the stub column specimens I-150×150×5-1 and I-150×150×5-2. With regards to the end section boundary conditions, the two end sections of each stub column FE model were fully restrained except for the longitudinal translation at one end, in order to mimic the fixed-ended boundary

condition adopted in the stub column tests. Initial local geometric imperfections were incorporated into the FE models, with the distribution patterns taken as the lowest elastic buckling mode shapes under compression and derived from a prior elastic eigenvalue buckling analysis [11,19,28,35–38]. Four initial local imperfection amplitudes, including the measured value ω_0, and 1/10, 1/30 and 1/100 of material thickness t, were employed to factor the imperfection patterns for the purpose of assessing the sensitivity of the FE models to imperfections and seeking the most suitable local geometric imperfection amplitudes to be utilised in the parametric studies.

3.3. Validation of finite element models

Upon development of the welded I-section stub column FE models, nonlinear Riks analysis [32] was conducted to determine the numerical failure loads, load–end shortening curves and failure modes, which were then compared against the corresponding experimentally derived results, allowing the accuracy of the developed numerical models to be examined. Table 6 reports the FE to test failure load ratios for the S690 welded I-section stub column specimens; the results of the comparison revealed that all the four considered initial local geometric imperfection amplitudes yield precise and consistent predictions of the experimental failure loads, while the best agreement between the experimental and numerical failure loads was generally acquired when the imperfection amplitude equal to 1/100 of the material thickness was utilised in the numerical simulation. Fig. 15 depicts a comparison between the experimental and numerical load–end shortening histories for a typical S690 welded I-section

stub column specimen I-140×70×5-1, where the full range of the experimental load–deformation response is shown to be well captured by numerical modelling. Moreover, the FE load–end shortening curve obtained from the stub column numerical model without incorporating membrane residual stresses is also plotted in Fig. 15, and shown to almost coincide with that derived from the numerical model with the membrane residual stresses included; this indicated that membrane residual stresses have an insignificant effect on the local stability and compression resistances of S690 high strength steel welded I-section stub columns. Excellent agreement was also obtained between the experimental and FE failure modes, as illustrated in Fig. 16. To conclude, the finite element models developed in Section 3.2 are capable of precisely simulating the stub column tests on S690 high strength steel welded I-sections, and thus considered to be validated.

3.4. Parametric studies

The validated S690 high strength steel welded I-section stub column FE models were adopted to carry out numerical parametric studies in this section, aiming at expanding the experimental data pool over a broader range of cross-section dimensions. In the present parametric studies, the average measured material properties of the longitudinal coupons, together with the initial local geometric imperfection amplitudes equal to 1/100 of the material thicknesses, were utilised. Regarding the geometric sizes of the modelled I-sections, the outer cross-section depths were fixed at 150 mm, while the flange widths were taken as 75 mm, 90 mm, 100 mm and 150 mm, respectively, leading to a wide spectrum of cross-section aspect ratios being

considered. The thicknesses of the flange and web of each modelled I-section were set to be equal and varied between 3 mm and 15 mm, resulting in a broad range of cross-section sizes being examined. The lengths of the stub column models were equal to the minimum of three times the outer section depths and twenty times the radii of gyration about the minor principal axes. In total, 90 numerical parametric study results for S690 welded I-section stub columns were derived.

4. Assessment of established international design codes

4.1. General

In this section, the experimental data, derived in Section 2, and the finite element results, obtained in Section 3, were utilised to assess the accuracy of the codified design provisions for S690 high strength steel welded I-section stub columns. Three established design standards, including the European code EN 1993-1-12 [12], American specification ANSI/AISC 360-16 [13] and Australian standard AS 4100 [14], were considered in the present study. The Eurocode EN 1993-1-12 [12] was developed specifically for high strength steels with grades greater than S460 up to S700, though mirroring most of the design provisions set out in EN 1993-1-1 [39] for normal strength mild steels, while the current ANSI/AISC 360-16 [13] and AS 4100 [14] provide design provisions for both normal strength mild steels and high strength steels with grades up to S690. With regards to the design of stub columns failing by local buckling, all the three considered design codes employ the cross-section classification framework and the

effective width method. In the following Section 4.2, the accuracy of the slenderness limits for classifications of the outstand flanges and internal webs of S690 welded I-sections, specified in the three design codes, was assessed, while the cross-section compression resistance predictions, particularly those for slender S690 welded I-section stub columns determined from the effective width formulations, were evaluated in Section 4.3.

4.2. Cross-section classification limits

All the three considered design standards, including the European code EN 1993-1-12 [12], American specification ANSI/AISC 360-16 [13] and Australian standard AS 4100 [14], adopt the cross-section classification framework for the design of S690 high strength steel welded I-sections subjected to compression. The American specification ANSI/AISC 360-16 [13] and Australian standard AS 4100 [14] categorise cross-sections in compression as non-slender and slender sections, where local buckling occurs upon and prior to the attainment of the material yield stress, respectively, with the corresponding cross-section compression resistances taken as the yield loads Af_y and effective compression resistances $A_{eff}f_y$, in which A and A_{eff} are respectively the gross area and effective area of the welded I-section. Four classes of cross-sections are defined in the European code EN 1993-1-12 [12]: Class 1, 2 and 3 sections (corresponding to the non-slender sections specified in ANSI/AISC 360-16 [13] and AS 4100 [14]) are capable of attaining the yield loads Af_y at failure, while Class 4 sections (corresponding to the slender sections specified in ANSI/AISC 360-16 [13] and AS 4100 [14]) fail before the material yield stress f_y is achieved, limiting the design cross-section compression

resistances to the effective compression resistances $A_{\text{eff}}f_{\text{y}}$. The class of a welded I-section subjected to compression is defined on the basis of its most slender constituent plate element, while each plate element (i.e. web or flange) is classified through comparing the flat width-to-thickness ratio (c_{w}/t or c_{f}/t) against the corresponding slenderness limits, in which c_{w} and c_{f} are the flat widths of the web and flange, respectively. Note that the slenderness limits between slender and non-slender plate elements are also known as Class 3 limits, yield slenderness limits and limiting width-to-thickness ratios in EN 1993-1-12 [12], ANSI/AISC 360-16 [13] and AS 4100 [14], respectively. Table 7 reports the slenderness limits between slender and non-slender outstand flanges (and internal webs), as specified in the three design codes, in which $\varepsilon_{\text{EC3}} = \sqrt{235/f_{\text{y}}}$, $\varepsilon_{\text{AISC}} = \sqrt{E/f_{\text{y}}}$ and $\varepsilon_{\text{AS}} = \sqrt{250/f_{\text{y}}}$ are the material parameters to reflect the difference in material strengths between high strength and normal strength steels, and $k_{\text{c}} = 4\sqrt{t/c_{\text{w}}}$ is a geometric coefficient to consider the effect of web size on the slenderness limit of flange.

The experimentally and numerically derived ultimate loads of S690 welded I-section stub columns are normalised with respect to the corresponding cross-section yield loads Af_{y}, and then plotted against the $c_{\text{f}}/(t\varepsilon_{\text{EC3}})$, $c_{\text{f}}/(t\varepsilon_{\text{AISC}}k_{\text{c}}^{0.5})$ and $c_{\text{f}}/(t\varepsilon_{\text{AS}})$ ratios of the flanges of the studied welded I-sections in Figs 17–19, respectively, together with the EC3, AISC and AS slenderness limits for non-slender/slender outstand flanges in compression. The results of the comparison generally revealed that the slenderness limits for non-slender/slender outstand flanges in compression, as specified in all of the three design standards [12–14], are safe and accurate when applied to S690 high strength steel welded I-sections. Similar graphic

comparisons are also presented in Figs 20–22 for the internal webs of the examined S690 welded I-sections, which also indicated the accuracy of the codified slenderness limits for non-slender/slender internal elements subject to compression. In summary, the slenderness limits, as given in the current EN 1993-1-12 [12], ANSI/AISC 360-16 [13] and AS 4100 [14], are safe and accurate for the plate element and cross-section classifications of S690 welded I-sections in compression.

4.3. Cross-section compression resistances

The accuracy of the cross-section compression resistance predictions of S690 welded I-section stub columns, as determined from EN 1993-1-12 [12], ANSI/AISC 360-16 [13] and AS 4100 [14], was assessed in this section. All the three design codes prescribe the use of the cross-section yield loads (Af_y) for non-slender (Class 1, 2 and 3) welded I-sections subject to compression, and employ the effective width methods for predicting the compressive load-carrying capacities of their slender (Class 4) counterparts. The effective width methods account for loss of effectiveness of each constituent plate element of a slender section susceptible to local buckling through a reduction in plate element width. The formulations for determining the (reduced) effective widths of slender internal and outstand plate elements, as specified in EN 1993-1-12 [12], ANSI/AISC 360-16 [13] and AS 4100 [14], are given by Eqs (3)–(5), respectively, where $\bar{\lambda}_1$ is the plate element slenderness and can be calculated from Eq. (6), in which c is the flat width of the plate element (taken as c_w and c_f for internal web and outstand flange of an I-section) and k_σ is the buckling factor, respectively taken as 4.0 and 0.43 for

internal and outstand plate elements in compression, and $\bar{\lambda}_{\mathrm{r,int}}$ and $\bar{\lambda}_{\mathrm{r,out}}$ are the AISC limiting width-to-thickness ratios for internal and outstand plate elements (see Table 7). Upon calculation of the effective width of each slender plate element of the welded I-section, the effective cross-section area (A_{eff}) and the effective compression resistance ($A_{\mathrm{eff}}f_{\mathrm{y}}$) can then be derived.

$$c_{\mathrm{eff,EC3}} = \begin{cases} c\left(\dfrac{1}{\bar{\lambda}_{\mathrm{l}}} - \dfrac{0.22}{\bar{\lambda}_{\mathrm{l}}^2}\right) \le c & \text{for internal elements} \\ c\left(\dfrac{1}{\bar{\lambda}_{\mathrm{l}}} - \dfrac{0.188}{\bar{\lambda}_{\mathrm{l}}^2}\right) \le c & \text{for outstand elements} \end{cases} \tag{3}$$

$$c_{\mathrm{eff,AISC}} = \begin{cases} c\left(\dfrac{1.31\bar{\lambda}_{\mathrm{r,int}}}{c/t} - \dfrac{0.31\bar{\lambda}_{\mathrm{r,int}}^2}{(c/t)^2}\right) \le c & \text{for internal elements} \\ c\left(\dfrac{1.49\bar{\lambda}_{\mathrm{r,out}}}{c/t} - \dfrac{0.49\bar{\lambda}_{\mathrm{r,out}}^2}{(c/t)^2}\right) \le c & \text{for outstand elements} \end{cases} \tag{4}$$

$$c_{\mathrm{eff,AS}} = \begin{cases} c\left(\dfrac{35}{c/(t\varepsilon_{\mathrm{AS}})}\right) \le c & \text{for internal elements} \\ c\left(\dfrac{14}{c/(t\varepsilon_{\mathrm{AS}})}\right) \le c & \text{for outstand elements} \end{cases} \tag{5}$$

$$\bar{\lambda}_{\mathrm{l}} = \frac{c/t}{28.4\varepsilon_{\mathrm{EC3}}\sqrt{k_{\sigma}}} \tag{6}$$

The experimental and numerical compressive load-carrying capacities of S690 welded I-section stub columns are normalised by the design cross-section compression capacities predicted from the three design codes, and then plotted against the c_{w}/t ratios of the I-sections, as shown in Figs 23–25, while Table 8 reports the mean test (and FE) to predicted cross-section compression resistance ratios $N_{\mathrm{u}}/N_{\mathrm{u,pred}}$ and the corresponding coefficients of variation (COVs).

The results of both the graphic and quantitative evaluations showed that all the three design codes yield rather accurate and consistent predictions of cross-section compressive load-carrying capacities for both slender and non-slender S690 welded I-section stub columns.

5. Conclusions

An experimental and numerical modelling programme has been carried out to investigate the material properties, membrane residual stresses and load-carrying capacities of S690 high strength steel welded I-section stub columns. The testing programme was performed on eight S690 welded I-sections, and included material tensile coupon tests, membrane residual stress and initial local geometric imperfection measurements, and sixteen concentrically loaded stub column tests. A new predictive model for membrane residual stress distributions in S690 welded I-sections was proposed. In conjunction with the experimental study, a finite element modelling investigation was also carried out, including a validation study, where FE models were developed and validated against the experimental results, and a parametric study, where the validated FE models were utilised to generate an extensive numerical data pool on S690 welded I-section stub columns. The obtained test and FE results were carefully analysed, and employed to assess the accuracy of the established slenderness limits for classifications of S690 high strength steel internal and outstand plate elements in compression and the local buckling design rules for S690 welded I-section stub columns, as given in EN 1993-1-12 [12], ANSI/AISC 360-16 [13] and AS 4100 [14]. The results of the assessment generally indicated that (i) all the three sets of codified slenderness limits between slender and non-slender outstand

(or internal) plate elements are safe and accurate when applied to S690 high strength steel welded I-sections in compression, and (ii) all the three design standards generally yield precise and consistent cross-section compression resistance predictions for both non-slender and slender S690 welded I-section stub columns.

Acknowledgements

The research work described in this paper is funded by the Regency Steel Asia (RSA) Endowment Fund. The authors are grateful to SSAB Swedish Steel Pte Ltd, Singapore for their help in the fabrication of S690 high strength steel welded I-section specimens. The assistance from Mr. Cheng Hoon Tui during the experiments and the financial support from NTU Research Scholarship are also gratefully acknowledged.

References

[1] Pocock G. High strength steel use in Australia, Japan and the US. Struct Eng 2006;84(21):27–30.

[2] Collin P, Johansson, B. Bridges in high strenght steel. Proceedings of IABSE Symposium Report. Budapest, Hungary; 2006;92:1–9.

[3] IABSE. Use and application of high-performance steels for steel structures. IABSE, ETH Zürich, Switzerland; 2005.

[4] Rasmussen KJR, Hancock GJ. Plate slenderness limits for high strength steel sections.

J Constr Steel Res 1992;23:73–96.

[5] Rasmussen KJR, Hancock GJ. Tests of high strength steel columns. J Constr Steel Res 1995;34:27–52.

[6] Shi G, Ban H, Bijlaard FSK. Tests and numerical study of ultra-high strength steel columns with end restraints. J Constr Steel Res 2012;70:236–47.

[7] Li T, Li G, Chan S, Wang Y. Behavior of Q690 high-strength steel columns: Part 1 : Experimental investigation. J Constr Steel Res 2016;123:18–30.

[8] Li T, Liu S, Li G, Chan S, Wang Y. Behavior of Q690 high-strength steel columns : Part 2 : Parametric study and design recommendations. J Constr Steel Res 2016;122:379–94.

[9] Ma T, Liu X, Hu Y, Chung K, Li G. Structural behaviour of slender columns of high strength S690 steel welded H-sections under compression. Eng Struct 2018;157:75–85.

[10] Ma T, Hu Y, Liu X, Li G, Chung K. Experimental investigation into high strength Q690 steel welded H-sections under combined compression and bending. J Constr Steel Res 2017;138:449–62.

[11] Ma T, Li G, Chung K. Numerical investigation into high strength Q690 steel columns of welded H-sections under combined compression and bending. J Constr Steel Res 2018;144:119–34.

[12] EN 1993-1-12:2007. Eurocode 3: design of steel structures – Part 1-12: Additional rules for the extension of EN 1993 up to steel grades S 700. Brussels: European Committee for Standardization (CEN); 2007.

[13] ANSI/AISC 360-16. Specification for the structural steel buildings. American Institute of Steel Construction (AISC); 2016.

[14] AS 4100-1998: Reconfirmed 2016. Steel structures. Australian standard, Committee BD-001; 2016.

[15] EN ISO 6892-1. Metallic matetials: tensile testing – Part 1: Method of test at room temperature. Brussels: European Committee for Standardization (CEN); 2016.

[16] Ziemian RD. Guide to stability design criteria for metal structures. 6th ed. John Wiley & Sons; 2010.

[17] Tebedge N, Alpsten G, Tall L. Residual-stress measurement by the sectioning method. Exp Mech 1973;13(2):88–96.

[18] Tebedge N, Tall L. Residual stresses in structural steel shapes – A summary of measured values. Fritz laboratory reports 74-12. Lehigh University; 1973.

[19] Sun Y, Zhao O. Material response and local stability of high-chromium stainless steel welded I-sections. Eng Struct 2019;178:212–26.

[20] Yuan H, Wang Y, Shi Y, Gardner L. Residual stress distributions in welded stainless steel sections. Thin-walled Struct 2014;79:38–51.

[21] ECCS. European convention for constructional steelwork: convention Europeenne de la construction metallique. 1976.

[22] BSK 99. Swedish regulations for steel structures. Boverkets handbok om stalkonstructioner. Karlskrona, Sweden; 1999.

[23] Schafer BW, Peköz T. Computational modeling of cold-formed steel: characterizing geometric imperfections and residual stresses. J Constr Steel Res 1998;47(3):193–210.

[24] Liang Y, Zhao O, Long Y, Gardner L. Stainless steel channel sections under combined compression and minor axis bending – Part 1 : Experimental study and numerical

modelling. J Constr Steel Res 2019;152:154–61.

[25] Zhao O, Rossi B, Gardner L, Young B. Experimental and numerical studies of ferritic stainless steel tubular cross sections under combined compression and bending. J Struct Eng (ASCE) 2016;142(2):04015110.

[26] Zhao O, Gardner L, Young B. Experimental study of ferritic stainless steel tubular beam-column members subjected to unequal end moments. J Struct Eng (ASCE) 2016;142(11): 04016091.

[27] Zhao O, Gardner L, Young B. Buckling of ferritic stainless steel members under combined axial compression and bending. J Constr Steel Res 2016;117:35–48.

[28] Zhao O, Rossi B, Gardner L, Young B. Behaviour of structural stainless steel cross-sections under combined loading – Part I: Experimental study. Eng Struct 2015;89:236–46.

[29] Center for Advanced Structural Engineering. Compression tests of stainless steel tubular columns. Investigation report S770. University of Sydney; 1990.

[30] Chen M, Young B. Material properties and structural behavior of cold-formed steel elliptical hollow section stub columns. Thin-walled Struct 2019;134:111–26.

[31] Chen M, Young B. Cross-sectional behavior of cold-formed steel semi-oval hollow sections. Eng Struct 2018;177:318–30.

[32] Hibbitt, Karlsson & Sorensen, Inc. ABAQUS/Standard user's Manual Volumes I-III and ABAQUS CAE Manual. Version 6.14. Pawtucket (USA); 2014.

[33] Hasham AS, Rasmussen KJR. Nonlinear analysis of locally buckled I-section steel beam-columns. Austra J Struct Eng 2002; 3(3): 171–200.

[34] Saliba N, Gardner L. Cross-section stability of lean duplex stainless steel welded I-sections. J Constr Steel Res 2013;80:1–14.

[35] Shi G, Zhou W, Bai Y, Lin C. Local buckling of 460 MPa high strength steel welded section stub columns under axial compression. J Constr Steel Res 2014;100:60–70.

[36] Wang Y, Li G, Chen S, Sun F. Experimental and numerical study on the behavior of axially compressed high strength steel columns with H-section. Eng Struct 2012;43:149–59.

[37] Zhang L, Tan KH, Zhao O. Experimental and numerical studies of fixed-ended cold-formed stainless steel equal-leg angle section columns. Eng Struct 2019;184:134–44.

[38] Liang Y, Vengadesh VJK, Zhang L, Zhao O. Flexural-torsional buckling behaviour of fi xed-ended hot-rolled austenitic stainless steel equal-leg angle section columns. J Constr Steel Res 2019;154:43–54..

[39] EN 1993-1-1:2005+A1:2014. Eurocode 3: design of steel structures – part 1.1: General rules and rules for buildings. Brussels: European Committee for Standardization (CEN); 2014.

Table 1

Average tensile material properties measured from longitudinal and transverse coupons.

Direction	E (MPa)	f_y (MPa)	f_u (MPa)	ε_u (%)	ε_f (%)	f_u/f_y
Longitudinal	216290	702.6	750.3	11	24	1.07
Transverse	201810	701.8	765.6	10	24	1.09

Table 2

Measured peak compressive and tensile residual stresses of S690 welded I-sections.

Specimen	Peak tensile residual stresses		Peak compressive residual stresses	
	Flange (f_{ft}/f_y)	Web (f_{wt}/f_y)	Flange (f_{fc}/f_y)	Web (f_{wc}/f_y)
I-200×100×5	0.48	0.38	-0.32	-0.28
	0.51		-0.36	
I-150×150×5	0.43	0.26	-0.30	-0.29
	0.53		-0.35	
Mean	0.49	0.32	-0.33	-0.29
Maximum	0.53	0.38	-0.36	-0.29

Table 3

Residual stress predictive models for S690 welded I-sections.

Predictive model	Peak tensile residual stresses	Peak compressive residual stresses	a	b	c	d
ECCS [21]	$1.0\,f_y$	$0.25\,f_y$	$0.05b_f$	$0.15b_f$	$0.075h_w$	$0.05h_w$
BSK 99 [22]	$1.0\,f_y$	From equilibrium	$0.75t_f$	$1.5t_f$	$1.5t_w$	$1.5t_w$
Proposed model	$0.8\,f_y$	From equilibrium	$0.225b_f$	$0.15b_f$	$0.075h_w$	$0.225h_w$

Note: b_f is the flange width; h_w is the clear distance between flanges;
t_w is the web thickness; t_f is the flange thickness.

Table 4

Measured geometric dimensions of S690 welded I-section stub columns.

Specimen ID	L (mm)	h (mm)	b_f (mm)	t (mm)	ω_w (mm)	ω_{f1} (mm)	ω_{f2} (mm)	ω_0 (mm)
I-50×50×5-1	149.5	47.74	49.39	4.88	0.04	0.05	0.04	0.05
I-50×50×5-2	149.1	49.51	49.38	4.88	0.03	0.03	0.03	0.03
I-70×70×5-1	206.7	68.71	69.15	4.97	0.10	0.07	0.09	0.10
I-70×70×5-2	207.3	68.20	69.09	4.96	0.07	0.03	0.06	0.07
I-80×60×5-1	239.8	79.98	60.02	5.00	0.03	0.09	0.08	0.09
I-80×60×5-2	239.9	80.01	59.94	4.99	0.13	0.08	0.06	0.13
I-90×70×5-1	265.6	90.00	69.19	5.00	0.05	0.05	0.04	0.05
I-90×70×5-2	265.5	89.87	69.12	4.97	0.05	0.06	0.04	0.06
I-100×100×5-1	299.9	99.35	98.87	4.89	0.07	0.10	0.12	0.12
I-100×100×5-2	296.1	99.22	98.97	4.99	0.07	0.11	0.10	0.11
I-140×70×5-1	298.9	139.39	69.14	5.00	0.08	0.04	0.04	0.08
I-140×70×5-2	300.0	139.36	69.03	4.99	0.07	0.09	0.07	0.09
I-150×150×5-1	450.0	149.86	149.02	4.91	0.11	0.10	0.14	0.14
I-150×150×5-2	448.5	149.78	149.01	4.95	0.09	0.12	0.10	0.12
I-200×100×5-1	417.2	199.49	99.43	4.96	0.10	0.08	0.07	0.10
I-200×100×5-2	417.5	199.37	99.35	4.98	0.11	0.07	0.07	0.11

Table 5

Summary of S690 welded I-section stub column test results.

Specimen ID	N_u (kN)	δ_u (mm)	$N_u/(Af_y)$
I-50×50×5-1	623.1	5.12	1.23
I-50×50×5-2	642.9	5.14	1.26
I-70×70×5-1	805.3	2.04	1.12
I-70×70×5-2	841.7	2.70	1.17
I-80×60×5-1	740.6	2.83	1.06
I-80×60×5-2	769.5	1.53	1.10
I-90×70×5-1	872.3	2.25	1.09
I-90×70×5-2	884.5	3.21	1.11
I-100×100×5-1	1127.3	1.53	1.10
I-100×100×5-2	1105.3	1.61	1.06
I-140×70×5-1	985.6	1.50	1.05
I-140×70×5-2	1023.8	1.46	1.09
I-150×150×5-1	1254.2	2.29	0.83
I-150×150×5-2	1274.6	1.67	0.84
I-200×100×5-1	1214.1	1.60	0.90
I-200×100×5-2	1155.4	1.35	0.85

Table 6

Comparison of stub column test results with finite element results for various imperfection amplitudes.

Specimen ID	FE N_u / Test N_u			
	Measured amplitude	t/10	t/30	t/100
I-50×50×5-1	0.90	0.85	0.88	0.90
I-50×50×5-2	0.90	0.85	0.87	0.89
I-70×70×5-1	0.97	0.91	0.95	0.98
I-70×70×5-2	0.95	0.90	0.93	0.95
I-80×60×5-1	0.96	0.92	0.95	0.97
I-80×60×5-2	0.92	0.90	0.92	0.94
I-90×70×5-1	0.93	0.88	0.91	0.93
I-90×70×5-2	0.91	0.87	0.89	0.91
I-100×100×5-1	0.93	0.89	0.92	0.94
I-100×100×5-2	0.96	0.91	0.95	0.97
I-140×70×5-1	0.97	0.92	0.95	0.98
I-140×70×5-2	0.94	0.89	0.92	0.94
I-150×150×5-1	0.99	0.96	0.98	1.00
I-150×150×5-2	0.98	0.95	0.97	0.99
I-200×100×5-1	0.95	0.92	0.94	0.96
I-200×100×5-2	1.00	0.96	0.99	1.01
Mean	0.95	0.91	0.93	0.96
COV	0.03	0.03	0.03	0.03

Table 7

Summary of EC3, AISC and AS slenderness limits between slender and non-slender plate elements in compression.

Design standard	Outstand flanges	Internal webs
EN 1993-1-12 [12]	$14\varepsilon_{EC3}$	$42\varepsilon_{EC3}$
ANSI/AISC 360-16 [13]	$0.64k_c^{0.5}\varepsilon_{AISC}$	$1.49\varepsilon_{AISC}$
AS 4100 [14]	$14\varepsilon_{AS}$	$35\varepsilon_{AS}$

Table 8

Comparisons of test and FE results with EC3, AISC and AS predicted compression resistances.

Cross-section category*	No. of test data	No. of FE data	$N_u/N_{u,EC3}$		$N_u/N_{u,AISC}$		$N_u/N_{u,AS}$	
			Mean	COV	Mean	COV	Mean	COV
Non-slender section	12	43	1.06	0.05	1.06	0.05	1.07	0.05
Slender section	4	47	1.05	0.03	1.02	0.01	1.10	0.05
Total	16	90	1.06	0.04	1.04	0.04	1.08	0.05

* The cross-section category is defined according to EN 1993-1-12 [12].

Fig. 1. Tensile coupon test setup.

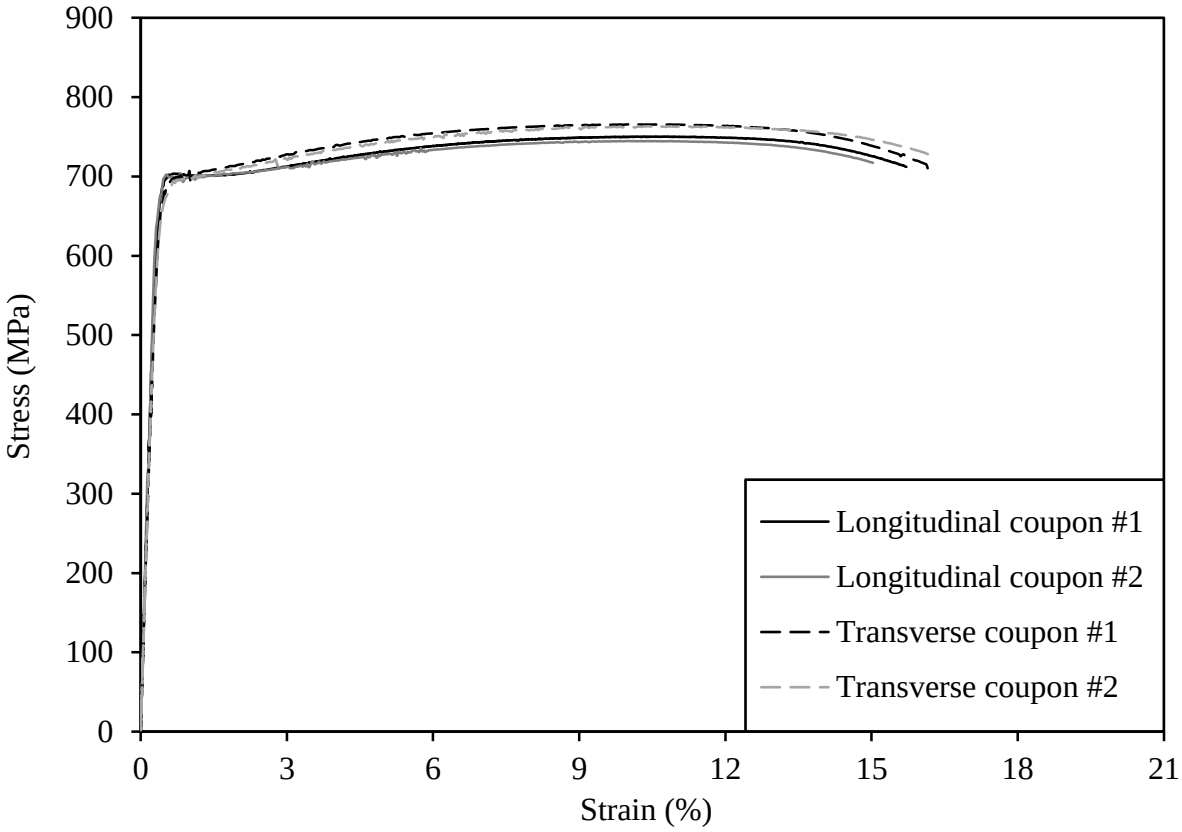

Fig. 2. Measured stress–strain curves from longitudinal and transverse coupons.

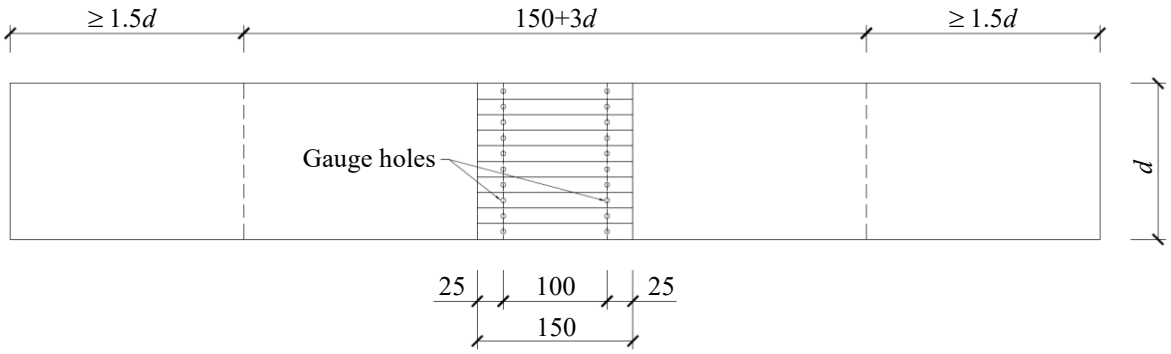

Fig. 3. Locations of strips cut for membrane residual stress measurements (dimensions in mm).

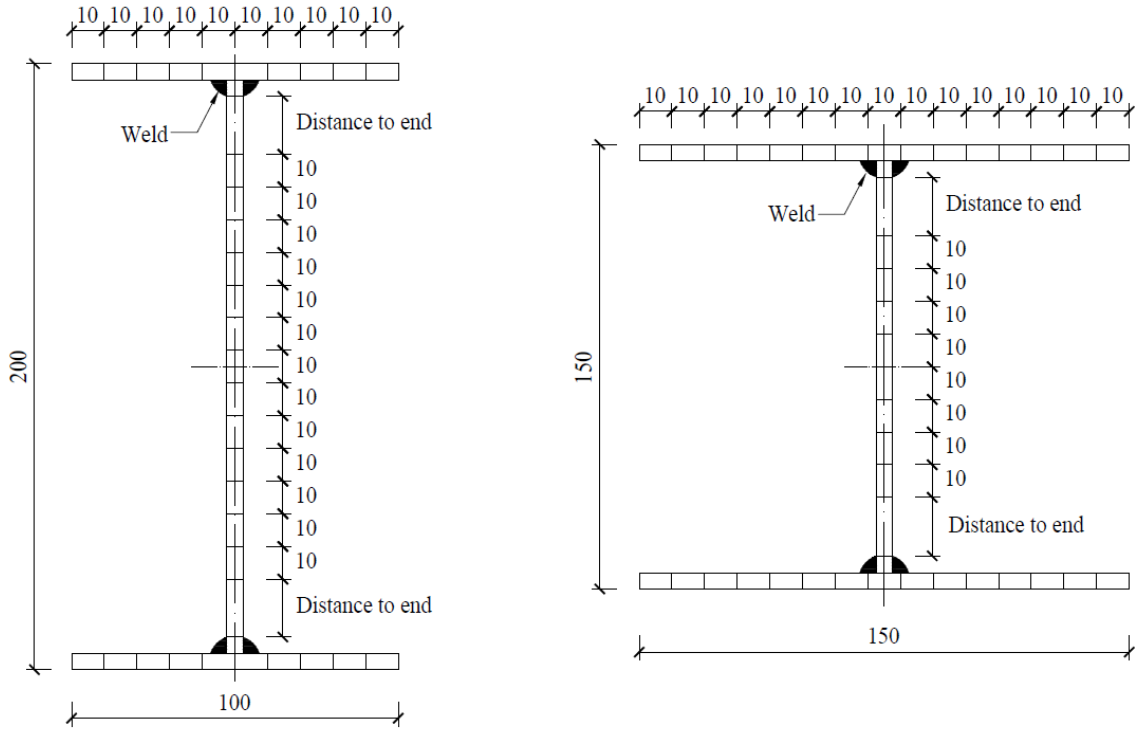

(a) I-200×100×5 (b) I-150×150×5

Fig. 4. Locations and dimensions of strips within I-sections (dimensions in mm).

Fig. 5. Typical sectioned S690 welded I-section I-200×100×5.

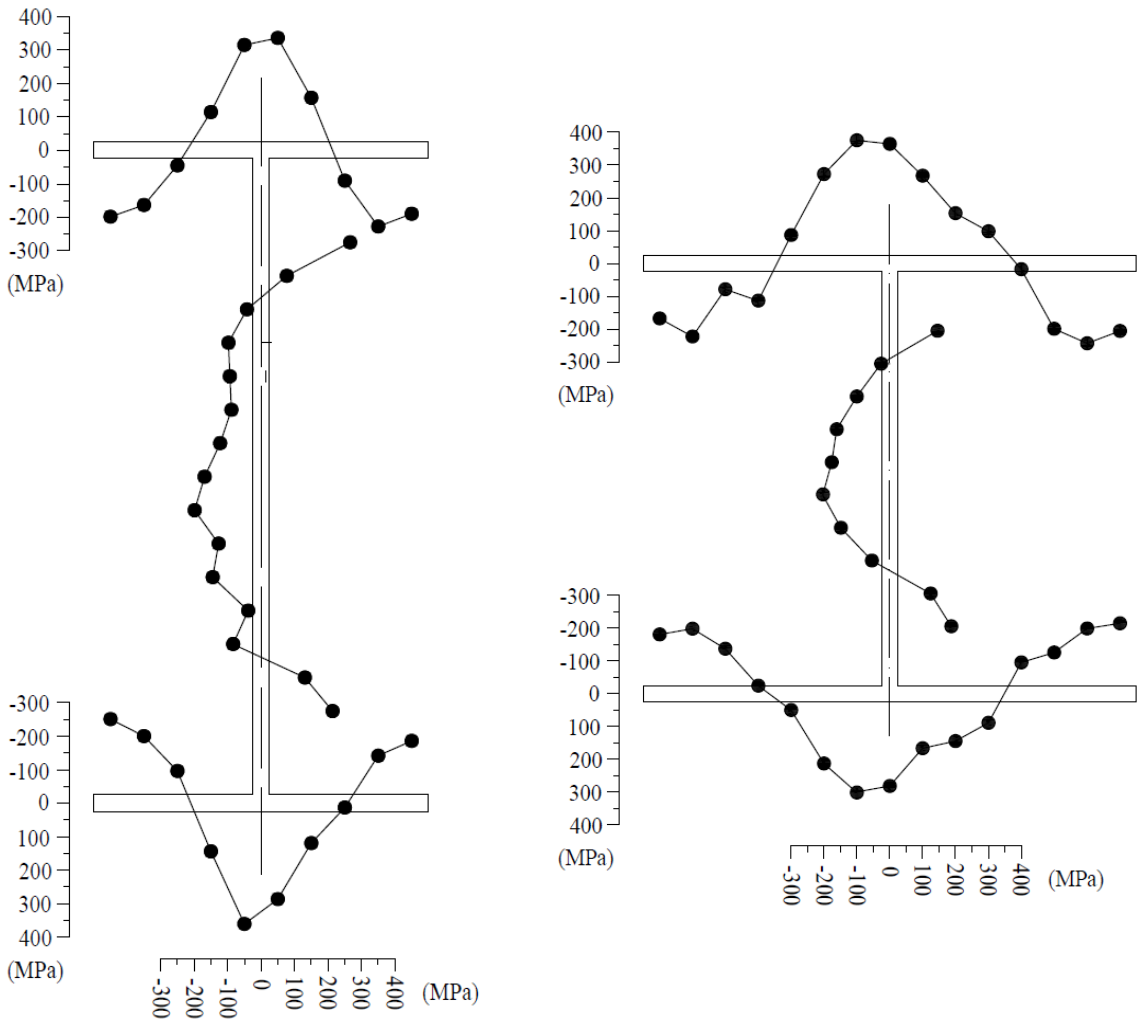

(a) I-200×100×5 (b) I-150×150×5

Fig. 6. Measured membrane residual stress patterns and amplitudes.

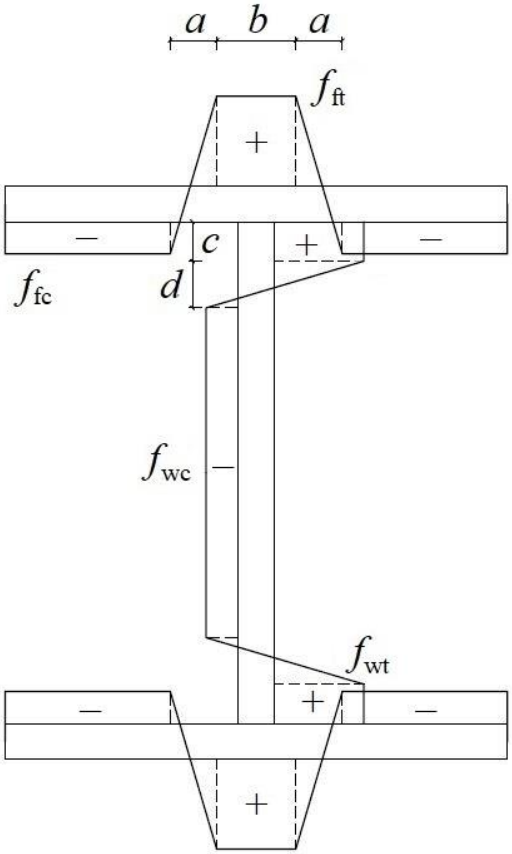

Fig. 7. General membrane residual stress pattern for welded I-sections.

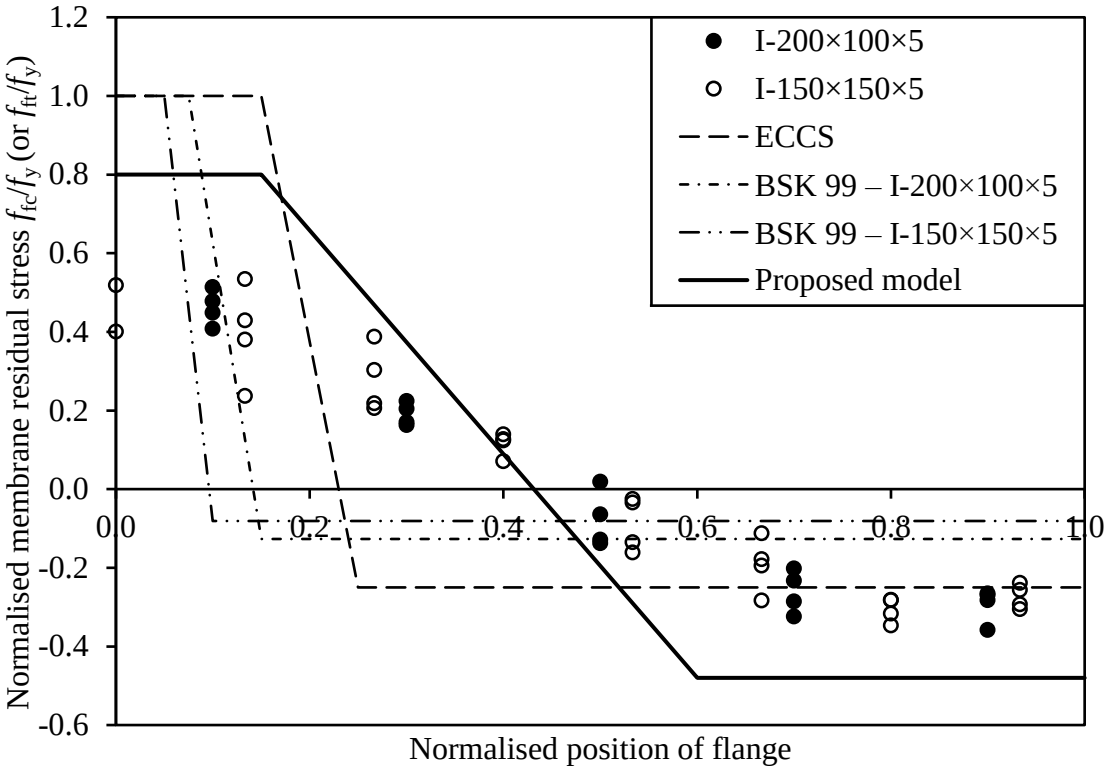

(a) flange

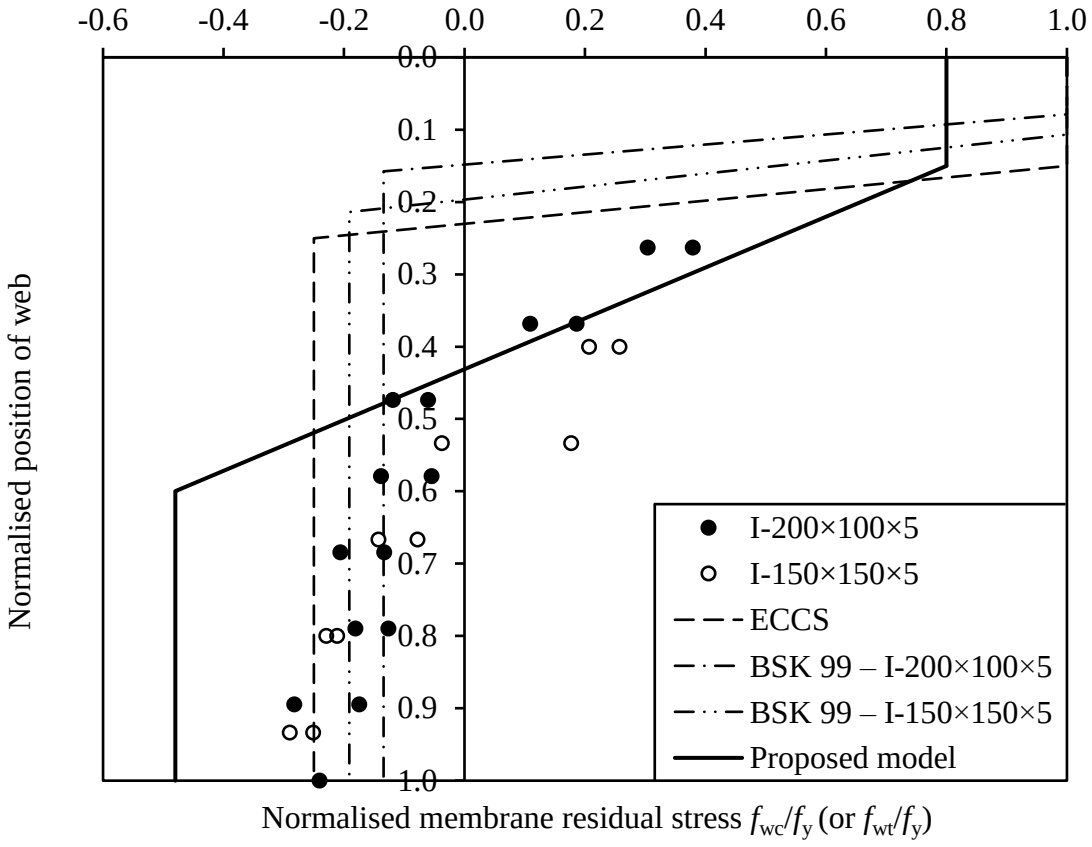

(b) web

Fig. 8. Comparisons between measured residual stress patterns and amplitudes and predictive models.

Fig. 9. Test rig for initial local geometric imperfection measurements.

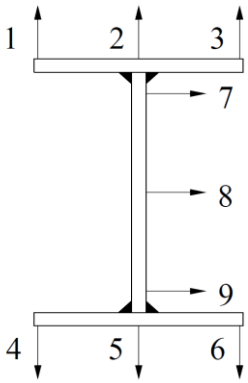

Fig. 10. Locations of initial local geometric imperfection measurements.

Fig. 11. Stub column test rig.

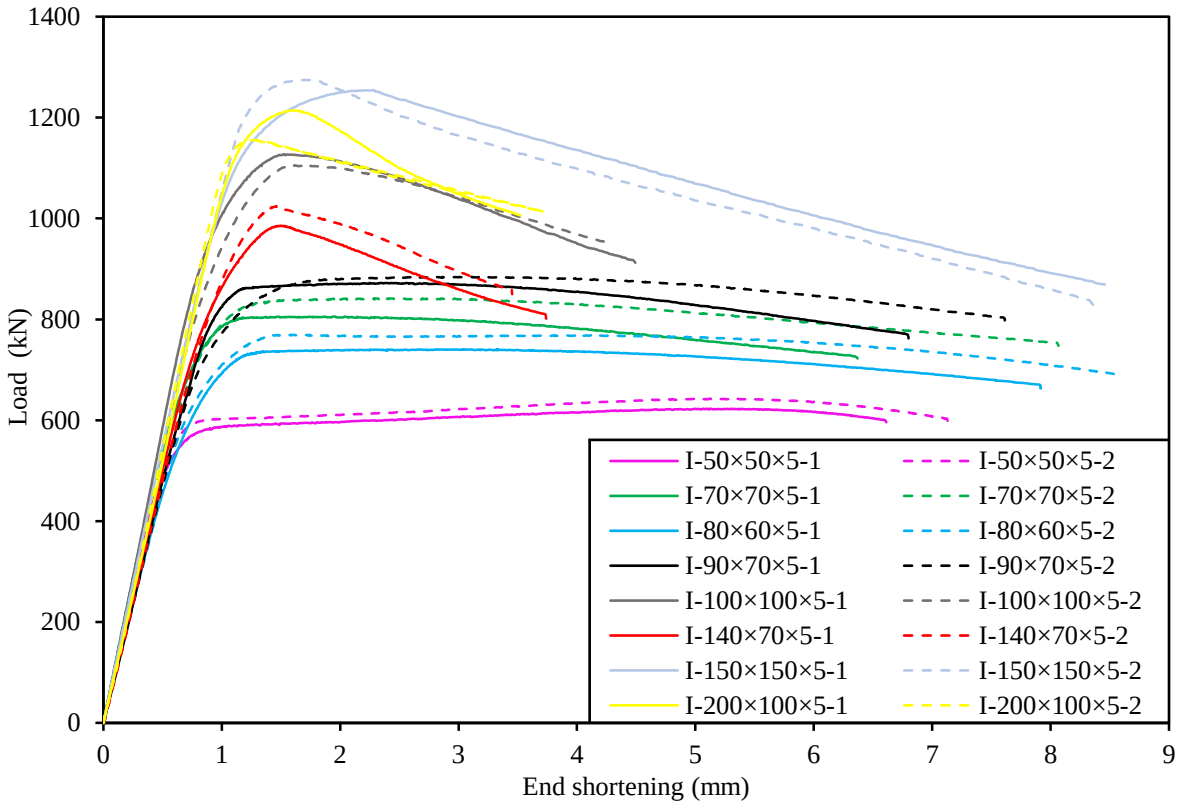

Fig. 12. Load–end shortening curves of S690 welded I-section stub column specimens.

Fig. 13. Failure modes of S690 welded I-section stub column specimens (from left to right: I-150×150×5-1, I-90×70×5-1, I-200×100×5-1).

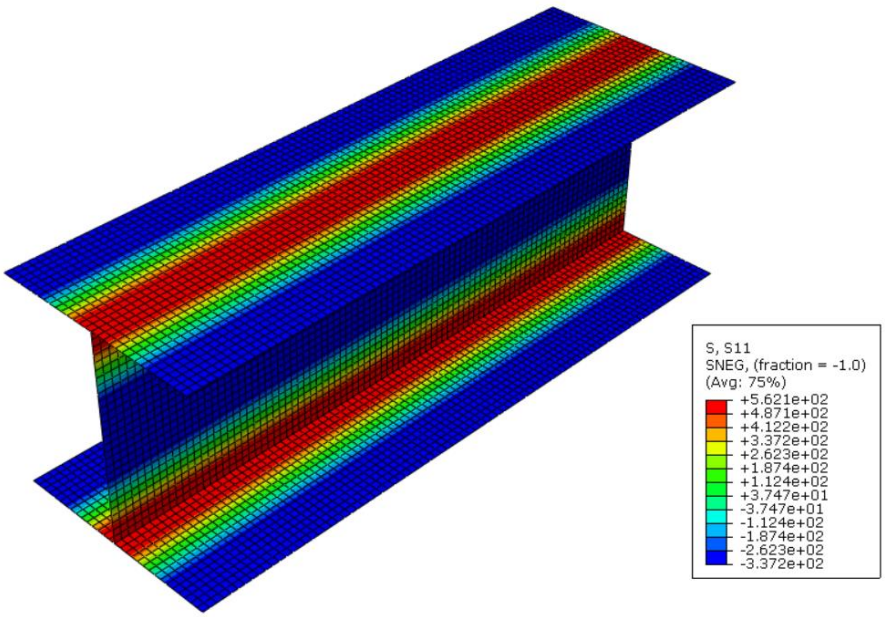

Fig. 14. Typical residual stress distribution (in MPa) in modelled S690 welded I-section I-150×150×5 (Positive values indicate tensile residual stresses while negative values indicate compressive residual stresses).

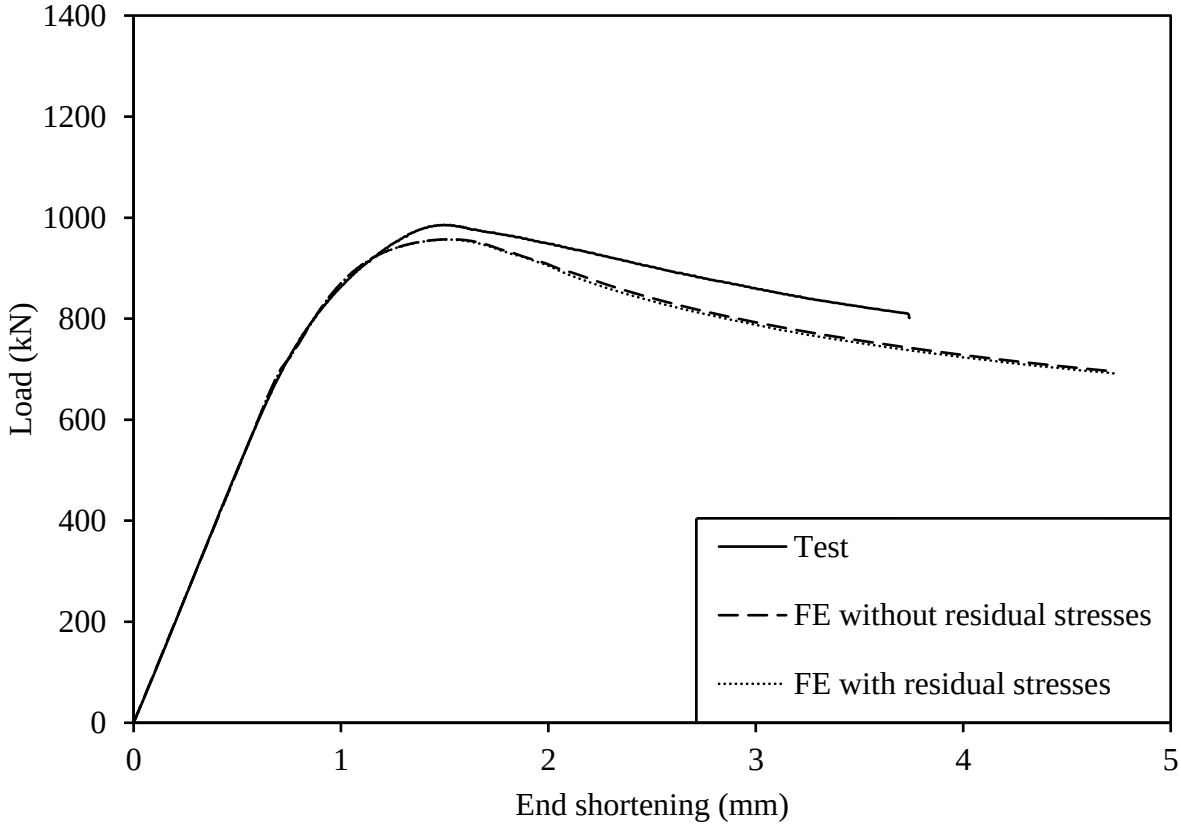

Fig. 15. Experimental and numerical load–end shortening curves for stub column specimen I-140×70×5-1.

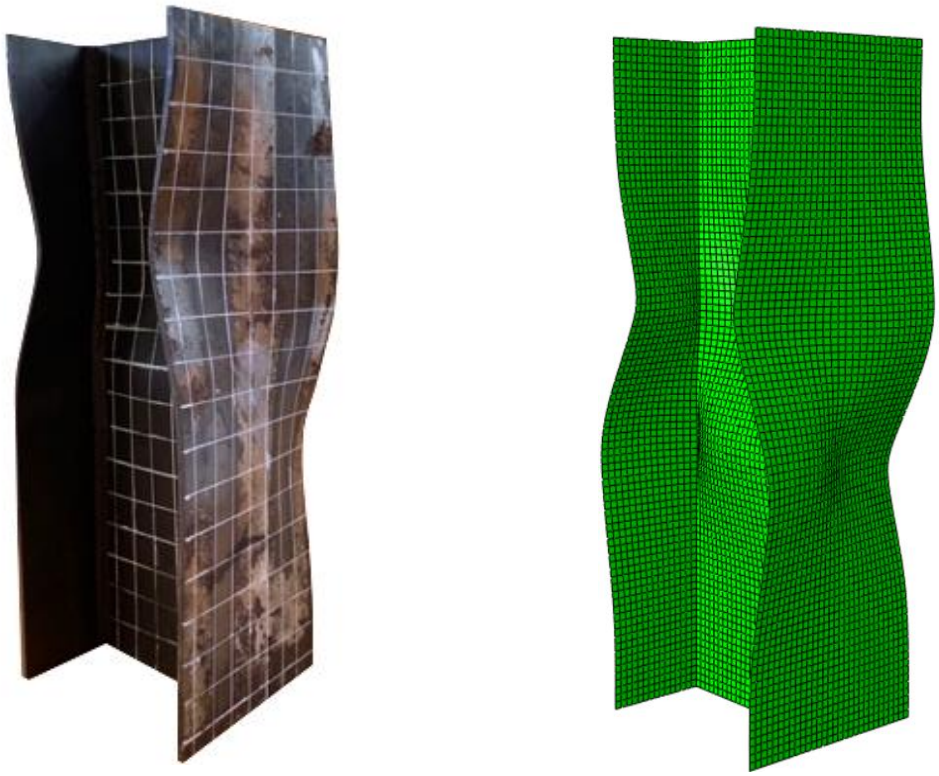

Fig. 16. Experimental and numerical failure modes for stub column specimen I-150×150×5-1.

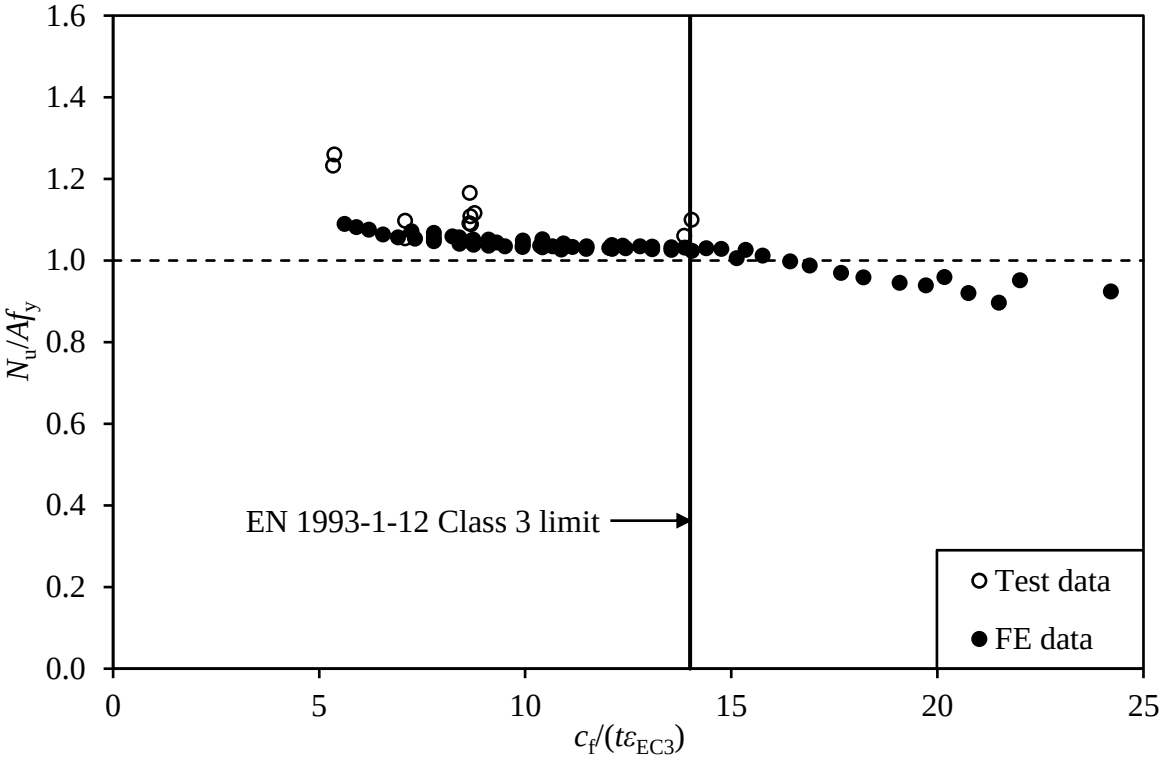

Fig. 17. EN 1993-1-12 Class 3 slenderness limit for outstand elements in compression.

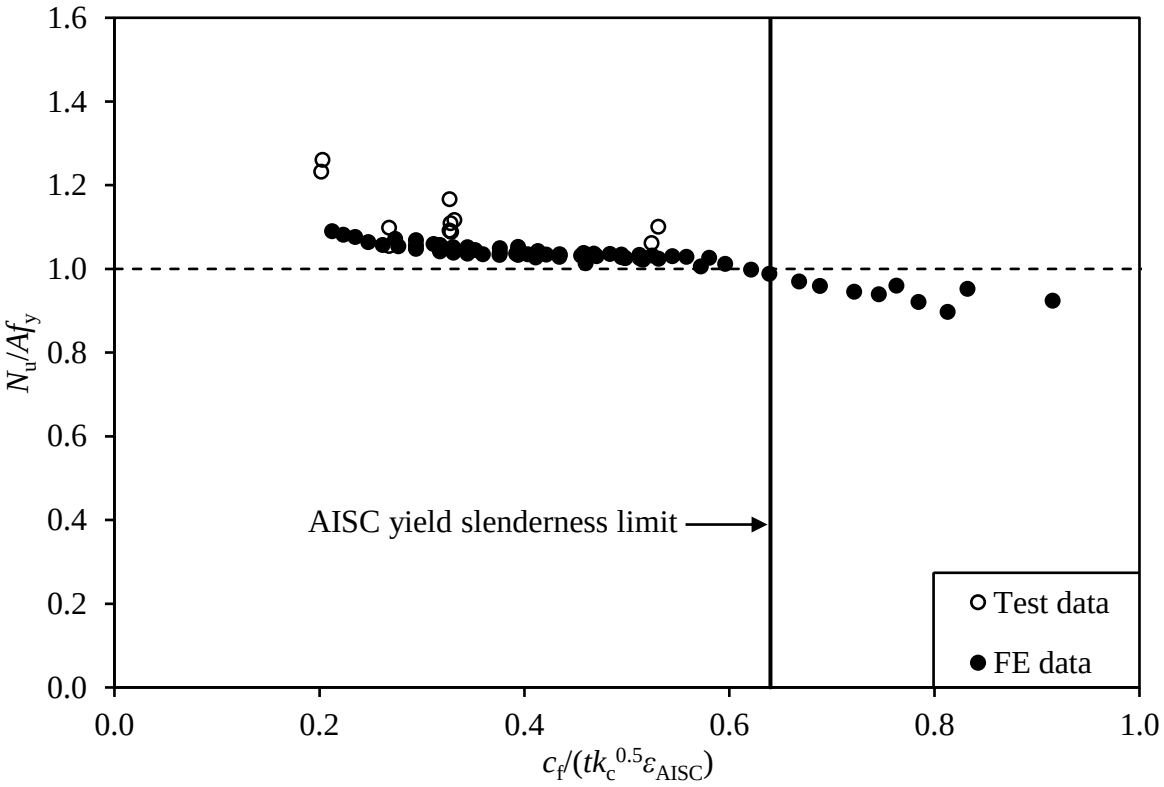

Fig. 18. ANSI/AISC 360-16 slenderness limit for outstand elements in compression.

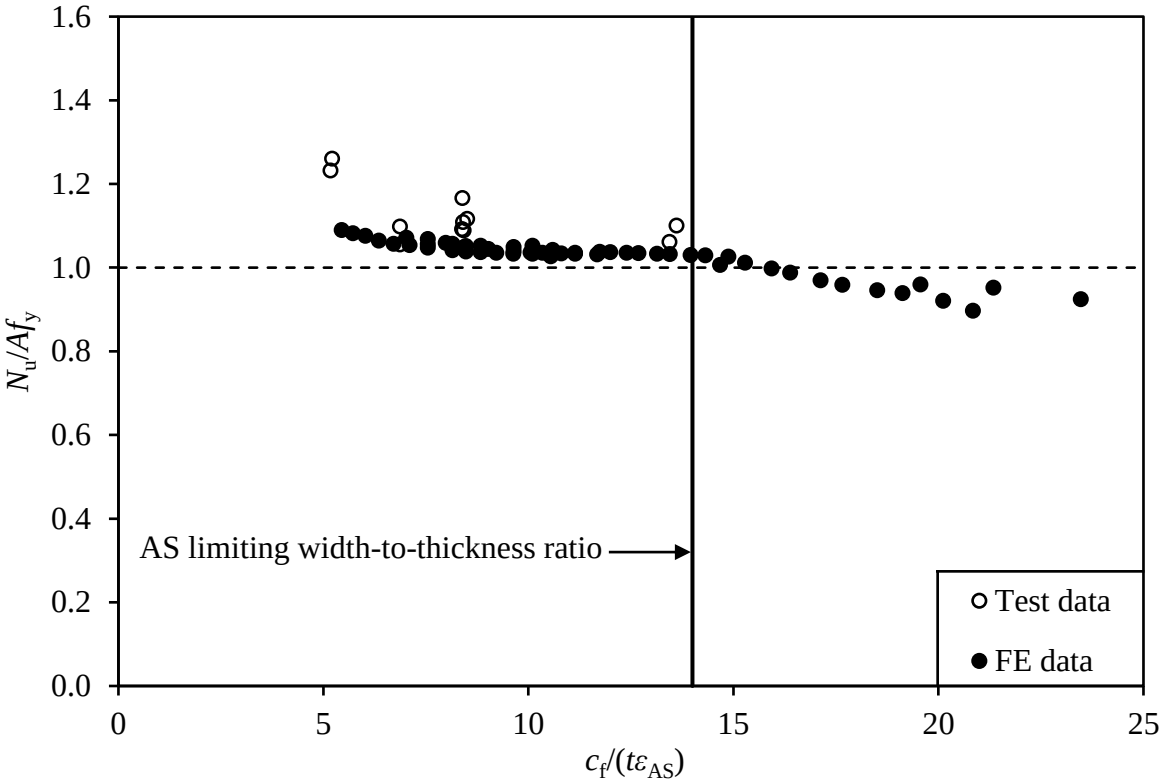

Fig. 19. AS 4100 slenderness limit for outstand elements in compression.

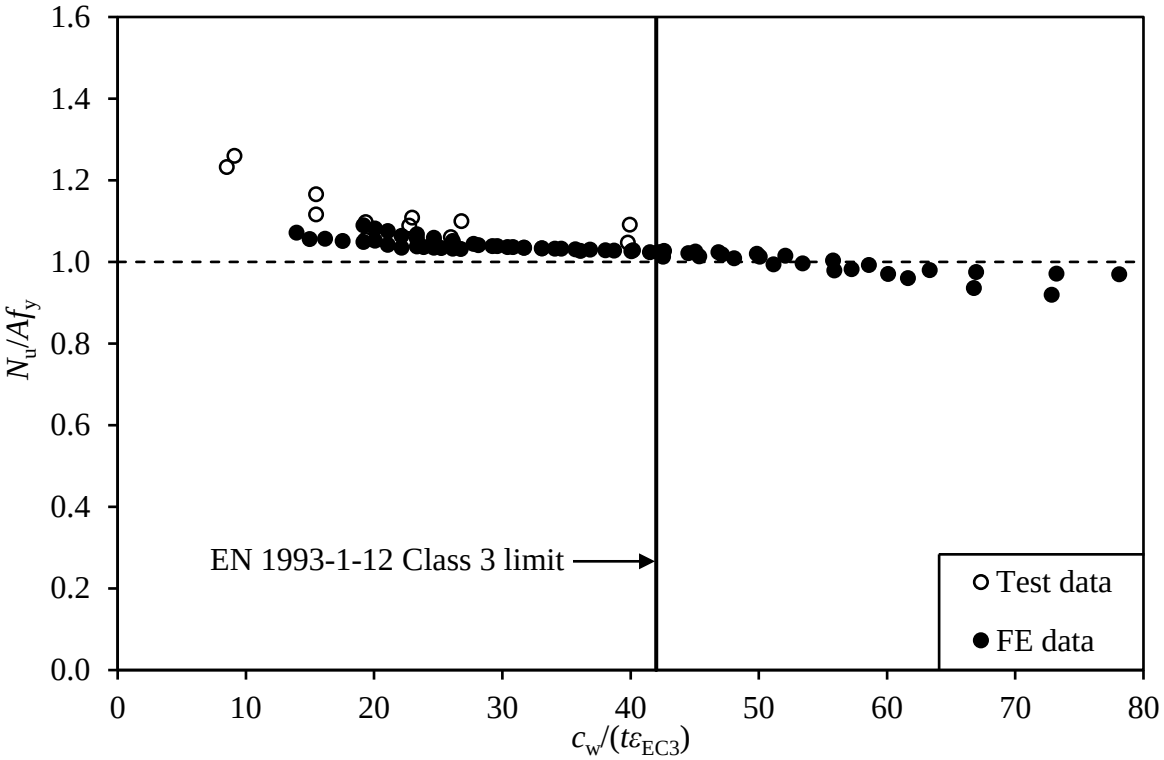

Fig. 20. EN 1993-1-12 Class 3 slenderness limit for internal elements in compression.

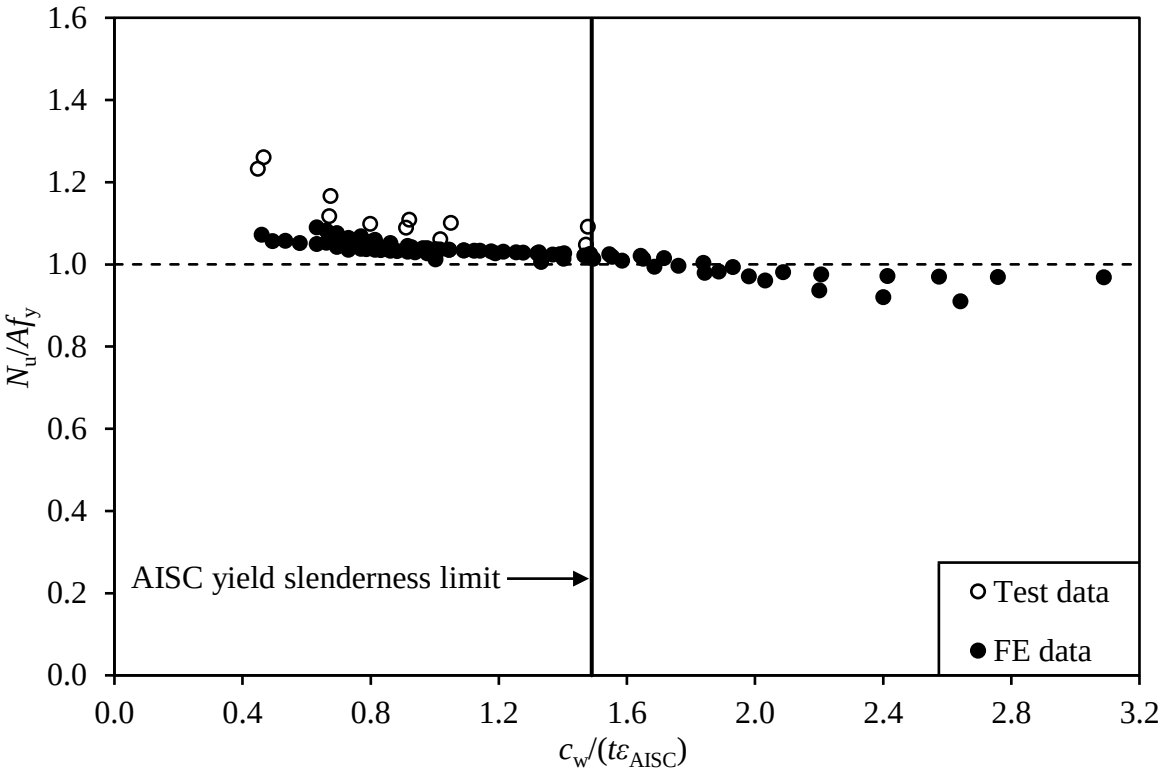

Fig. 21. ANSI/AISC 360-16 slenderness limit for internal elements in compression.

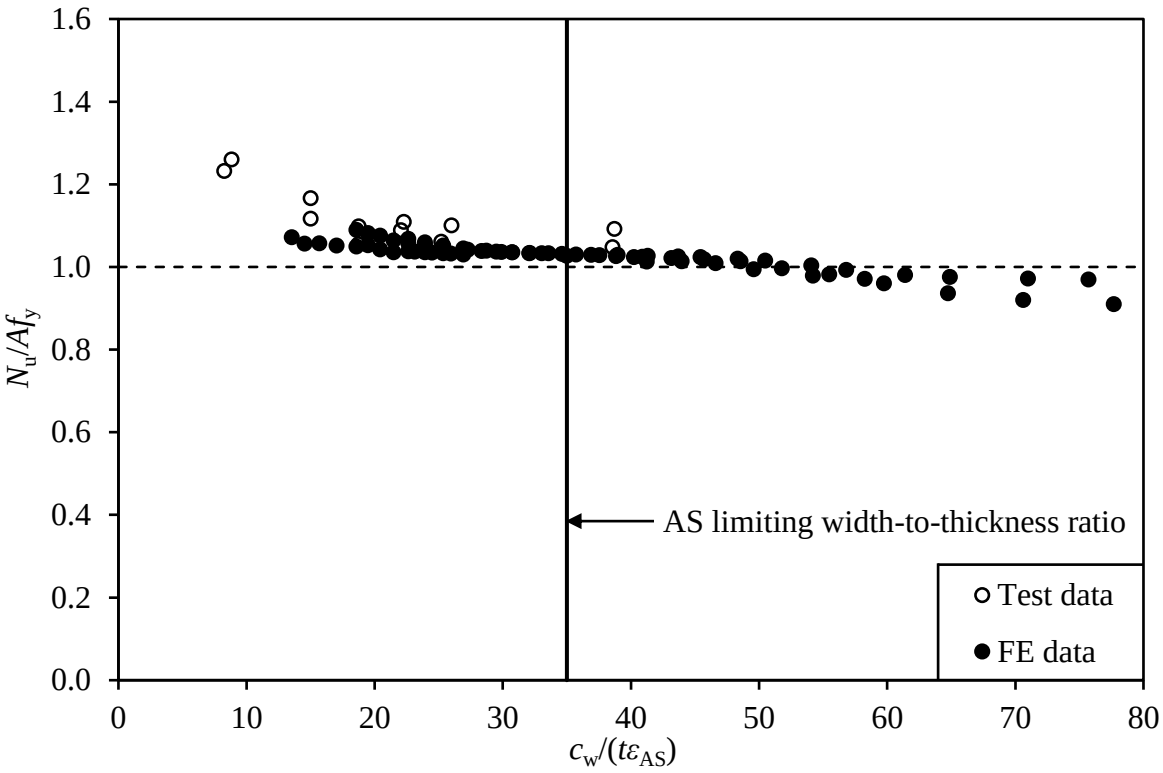

Fig. 22. AS 4100 slenderness limit for internal elements in compression.

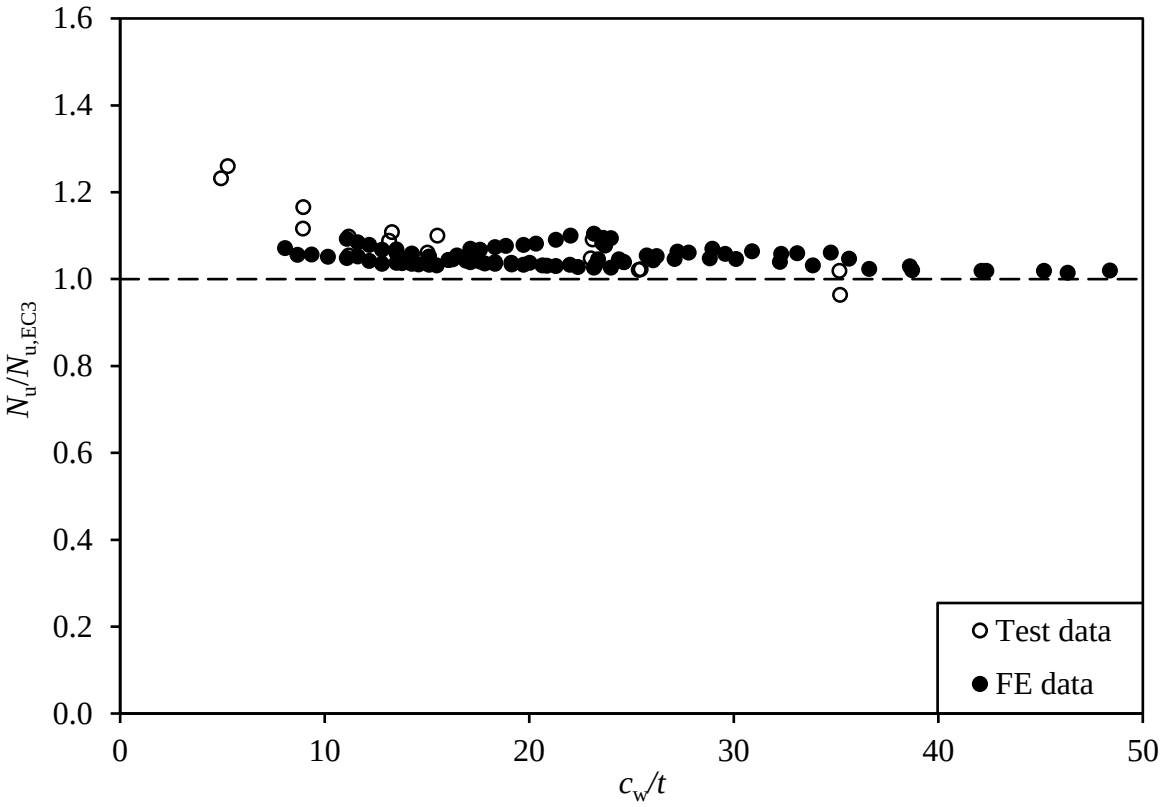

Fig. 23. Comparison of experimental and numerical results with EC3 resistance predictions.

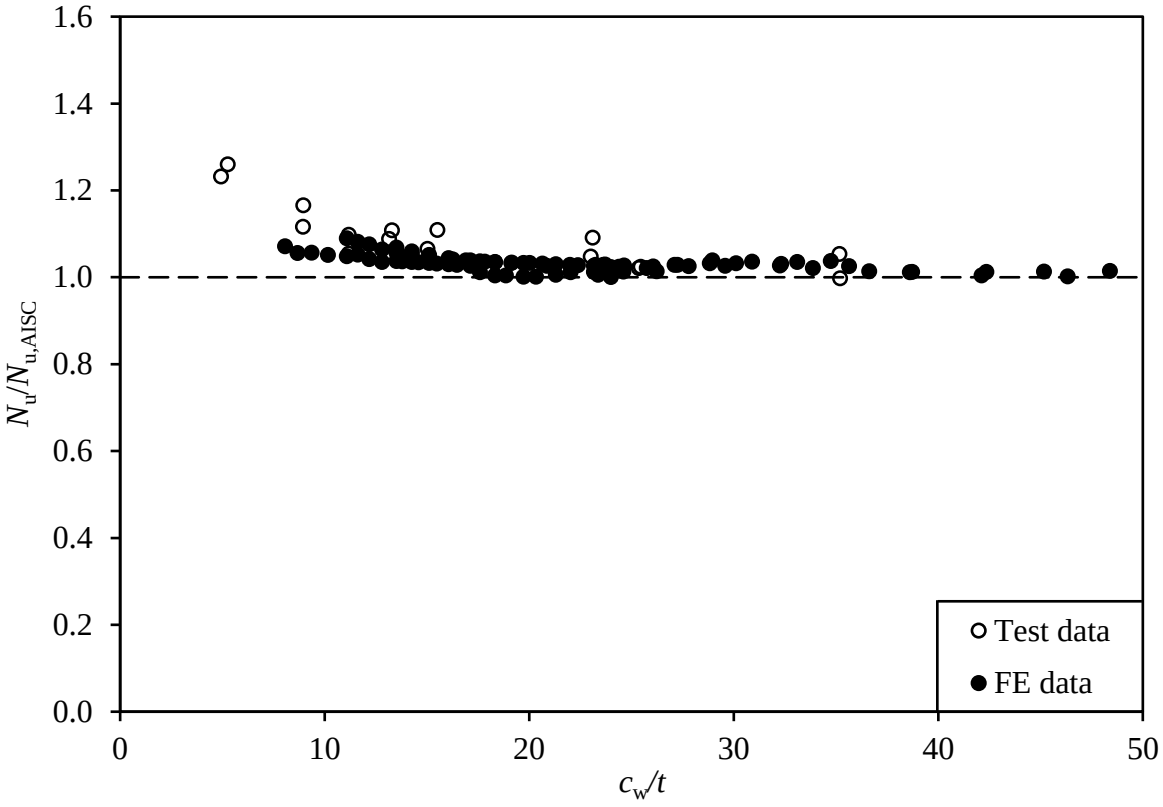

Fig. 24. Comparison of experimental and numerical results with AISC resistance predictions.

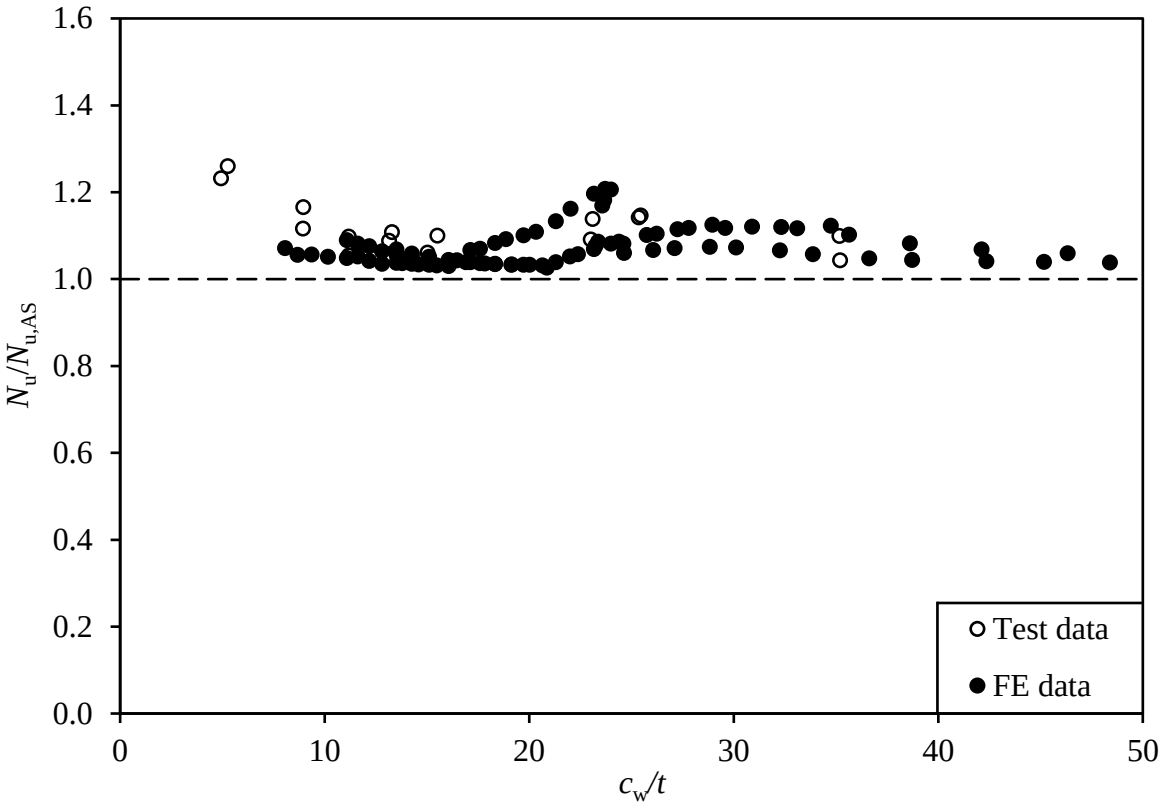

Fig. 25. Comparison of experimental and numerical results with AS resistance predictions.